Control of Charge Dilution in Turbocharged Diesel Engines via Exhaust Valve Timing

Hakan Yilmaz

Anna Stefanopoulou

Department of Mechanical Engineering,
University of Michigan,
Ann Arbor, MI 48109

In this paper we extend an existing crank angle resolved dynamic nonlinear model of a six-cylinder 12 l turbocharged (TC) Diesel engine with exhaust valve closing (EVC) variability. Early EVC achieves a high level of internal exhaust gas recirculation (iEGR) or charge dilution in Diesel engines, and thus reduces generated oxides of nitrogen (NO_x). This model is validated in steady-state conventional (fixed EVC) engine operating points. It is expected to capture the transient interactions between EVC actuation, the turbocharger dynamics, and the cylinder-to-cylinder breathing characteristics, although this has not been explicitly validated due to lack of hardware implementation. A nominal low order linear multi-input multi-output model is then identified using cycle-sampled or cycle-averaged data from the higher order nonlinear simulation model. Various low-order controllers that vary EVC to maximize the steady-state iEGR under air-to-fuel ratio (AFR) constraints during transient fueling demands are suggested based on different sensor sets. The difficulty in the control tuning arises from the fact that the EVC affects both the AFR and engine torque requiring coordination of fueling and EVC. Simulation results are shown on the full order model. [DOI: 10.1115/1.1985440]

1 Introduction

Diesel or compression ignition direct injection (CIDI) engines face increasingly stringent emission regulations. One type of these regulated pollutants is associated with oxides of nitrogen (NO_x). NO_x emissions correlate with peak cylinder temperature [1,2]. Diluting the combustion mixture with recirculated exhaust gas (burned gas+ oxygen) increases the trapped cylinder gas mass for a given air-to-fuel ratio (AFR). The larger mass from this dilution yields larger heat capacity and lower peak combustion temperature. Exhaust gas recirculation (EGR) can therefore be used to reduce the NO_x emissions. With proper control, reduced NO_x levels can be achieved without significant power and particulate emissions penalties. Thus, EGR is considered by most heavy duty Diesel engine manufacturers. Moreover, in homogeneous charge compression ignition (HCCI) engines a high level of EGR can be used to indirectly control combustion initiation. Consequently, achieving fast and accurate control of EGR is an important objective for conventional Diesel and HCCI engines [3,4].

Conventional external EGR (eEGR), relies on a pressure drop from exhaust manifold to intake manifold. The flow of eEGR is typically regulated by the EGR valve. Well-tuned and highly efficient CIDI engines often operate under conditions where the intake manifold pressure is higher than the exhaust manifold pressure. Such engines require additional hardware for achieving external EGR, such as a Venturi system, intake EGR throttle, variable geometry turbocharger, or exhaust backpressure valve (see Fig. 1). All these mechanisms have either limited range of operation or achieve the required EGR level by throttling the intake or exhaust flow, and therefore, reducing the efficiency of turbocharged CIDI engines. Moreover, these mechanisms do not allow fast control of in-cylinder AFR during fueling transients because cylinder charge is controlled indirectly through the turbocharger and the intake manifold [1,5]. The system dynamics is, thus, limited by the intake and exhaust manifold filling and turbocharger dynamics.

Internal exhaust gas recirculation (iEGR) is an alternative method for achieving EGR and can avoid losses that are associated with pumping exhaust gas from the exhaust manifold to the intake manifold through an eEGR valve [6]. By employing variable valve timing (VVT), an iEGR approach can achieve to the dilution level by early exhaust valve closing (eEVC), late exhaust valve closing (lEVC), or reopening on the induction stroke [7]. In this work, due to piston geometry limitations, eEVC is selected as the VVT degree of freedom to achieve EGR control. Using a crank angle based, nonlinear, dynamic model of a direct-injection, turbocharged Diesel engine, we examine the potential of a VVT-regulated iEGR for future engine applications. Transient and steady-state response of the engine with VVT is analyzed using the high order nonlinear model, and these results are used to create lower order linear models and feedforward control laws. Feedback controllers are then designed for the transient control of EVC during fueling transients. We show that controlling EVC achieves a good level iEGR and allows very fast AFR response when compared to the conventional (fixed EVC).

Apart from the Diesel application specific results, we also derive a family of simple linear time-invariant multiple-input multiple-output (MIMO) models similarly to Ref. [8] and controllers that can be used for control design and evaluation of transient engine performance. We anticipate that this study and methodology will be a useful example for VVT engine development. A seamless integration of engine model development and control design is necessary for successful integration of many new valve actuators and variable valve timing strategies in future vehicles.

2 Crank Angle Resolved Model

In a multicylinder application, variable valve timing modulates the interactions between the various cylinders and the manifolds that connect them (see Fig. 2) resulting in a complex nonlinear system. We employ the standard spatially averaged, zero-dimensional modeling techniques similar to Refs. [9] and [10] because they have been successfully applied in other VVT control schemes [11]. We develop a nonlinear crank angle resolved dynamic model of mass and heat flows in which cylinder volumes are considered individually and intake and exhaust manifolds are lumped into volumes that are coupled to the cylinders and to each

Contributed by the Dynamic Systems, Measurement, and Control Division of THE AMERICAN SOCIETY OF MECHANICAL ENGINEERS for publication in the ASME JOURNAL OF DYNAMIC SYSTEMS, MEASUREMENT, AND CONTROL. Manuscript received: April 10, 2003. Final revision: August 24, 2004. Associate Editor: Andrew Alleyne.

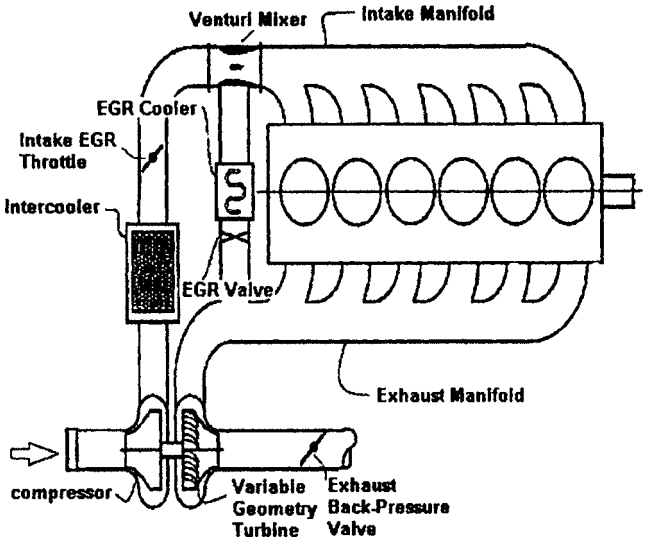

Fig. 1 Current external EGR applications: Venturi mixer, intake EGR throttle, variable geometry turbocharger, exhaust backpressure valve

other. Each component includes three state variables representing the mass, the pressure, and the burned gas fraction of the respective component. The differential equations for the state variables are derived from the ideal gas law, conservation of energy, conservation of mass, and an assumption that each component is a plenum with homogeneous temperature, pressure and density. The torque (Tq) produced at the crankshaft is calculated based on the individual cylinder pressure and piston motion using the idealized slider-crank mechanism.

The resulting model has 29 crank angle resolved states. We augment the model with additional states that correspond to the integrators for the cycle averaged variables. This model has been initially developed for control of compression braking (secondary exhaust valve opening during the compression stroke) in Ref. [12], presented in Ref. [13], and used consequently to design longitudinal speed controllers in Refs. [14] and [15]. Here the model has been augmented with exhaust valve closing variability and states for burned gas fraction. This model has been validated in steady-state conventional (no VVT) engine operating points in Refs. [13] and [15]. It is expected to capture the transient interactions between VVT actuation, the turbocharger dynamics, and the cylinder-to-cylinder breathing characteristics, although this has not been explicitly validated due to the lack of hardware implementation. We present in the next sections a summary of the model with emphasis on the additional burned gas fraction states introduced by the EVC variability.

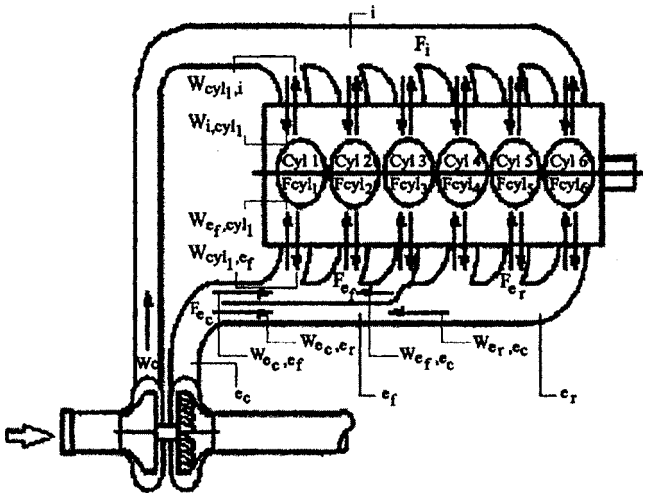

Fig. 2 Notations of control volumes and gas flows

A summary of the nomenclature in the modeling sections follow. Variables associated with mass are denoted with m in kilograms, mass flow rates from x volume to y volume are denoted with $W_{x,y}$ in kilograms per second, pressures with p in kiloPascal, temperature with T in Kelvin, burned gas fractions with F (unitless), torque with T_q in Nm, power with P in kW, engine speed with N in rpm, efficiencies with η (unitless), volumes with V in m^3. The subscript c denotes variables associated with the compressor, t relates to turbine variables, tc relates to turbocharger, cyl_j relates to jth cylinder, i relates to intake manifold, e_f relates to front exhaust manifold, e_r relates to the rear exhaust manifold, and e_c and relates to the collector manifold.

2.1 Cylinder States. The cylinders are modeled as plenums with homogeneous pressure and temperature distributions. For the first three cylinders, gas exchange takes place between the front exhaust manifold (e_f) and the jth cylinder (cyl_j), so the mass balance becomes

$$dm_{cyl_j}/dt = W_{i,cyl_j} + W_{e_f,cyl_j} + W_{f_{cyl_j}} - W_{cyl_j,i} - W_{cyl_j,e_f}, \quad (1)$$

where $W_{f_{cyl_j}}$ is the fuel flow rate into the jth cylinder, which we assume is injected in the cylinder within the injection pulse width (δ in degrees) following the start of injection (SOI) timing. Specifically, $W_{f_{cyl_j}} = W_f \Delta T/(6\delta)$, where W_f is the cycle-averaged fuel flow, ΔT is the cycle duration, and δ is the duration of the injection pulse width in degrees. The injection pulse width is defined by the engine manufacturer and is modeled with a second order polynomial of engine speed and cycle-averaged fuel flow. The flows $W_{x,y}$ from x volume to y volume are defined in Sec. 2.6. Note that we account for possible backflow from the jth cylinder to the intake manifold and from the front exhaust manifold to the jth cylinder by explicitly subtracting $W_{cyl_j,i}$ and adding W_{e_f,cyl_j} from the mass balance equation.

The pressure state equations for the cylinder states include the cylinder volume as a function of crank angle and also a heat release description modeled by

$$dp_{cyl_j}/dt = \gamma(RT_i W_{i,cyl_j} - RT_{cyl_j} W_{cyl_j,i} - RT_{cyl_j} W_{cyl_j,e_f} + RT_{e_f} W_{e_f,cyl_j} - \dot{V}_{cyl_j} p_{cyl_j})/V_{cyl_j} + (\gamma - 1) W_{afb_j} Q_{lhv}/V_{cyl_j}, \quad (2)$$

where the apparent fuel burnt, W_{afb_j} is defined in Sec. 2.5 The temperatures in the control volumes are calculated based on the mass and pressure states and the ideal gas law.

Additionally, in order to understand the amount of iEGR achieved, another state, burned gas fraction, is defined as the ratio of the mass of the burned gas (m_{bg}) to the mass of the total gas (m_{total}) in the prescribed control volume

$$F = m_{bg}/m_{total}. \quad (3)$$

Taking the time derivative of the equation above gives the rate of change of burned gas fraction, which describes the required state equation

$$dF/dt = (\dot{m}_{bg} m_{total} - m_{bg} \dot{m}_{total})/(m_{total})^2 = (\dot{m}_{bg} - F\dot{m}_{total})/m_{total}. \quad (4)$$

Accordingly, for the first three cylinders, the burned gas fraction can be defined using the mass balance described by Eq. (1) and the component balance formed as

$$dm_{\mathrm{bg}_{\mathrm{cyl}_j}}/dt = W_{i,\mathrm{cyl}_j}F_i + W_{e_f,\mathrm{cyl}_j}F_{e_f} + (1+\mathrm{AFR}_s)W_{\mathrm{afb}_j}\alpha_{f_j} - W_{\mathrm{cyl}_j,i}F_{\mathrm{cyl}_j} - W_{\mathrm{cyl}_j,e_f}F_{\mathrm{cyl}_j}, \quad (5)$$

where AFR_s is the stoichiometric air to fuel ratio and α_{f_j}, which is defined in Sec. 2.5 scales the apparent fuel burnt to match the total fuel injected and burnt in the cylinder. Substituting Eqs. (1), (3), and (5) in Eq. (4) provides the burned gas mass state equation for cylinder j

$$dF_{\mathrm{cyl}_j}/dt = ((1+\mathrm{AFR}_s)\alpha_{f_j}W_{\mathrm{afb}_j} + W_{i,\mathrm{cyl}_j}(F_i - F_{\mathrm{cyl}_j}) + W_{e_f\mathrm{cyl}_j}(F_{e_f} - F_{\mathrm{cyl}_j}) - W_{f_{\mathrm{cyl}_j}}F_{\mathrm{cyl}_j})/m_{\mathrm{cyl}_j} \quad (6)$$

where the injected fuel rate $W_{f_{\mathrm{cyl}_j}}$ and the scaled apparent fuel burnt W_{afb_j} are used in (5) and (6) to model accurately the crank angle resolved changes of the F_{cyl_j}. Note here that the injected fuel is a pulse of magnitude $W_{f_{\mathrm{cyl}_j}}$ and duration equal to the injection pulse width δ, whereas the fuel burnt $\alpha_{f_j}W_{\mathrm{afb}_j}$ has a double-bell shape shifted from the injection timing as shown in Fig. 3 and discussed in Sec. 2.5. The control output used in Sec. 3.1 is the sampled F_{cyl_j} just before the SOI. The AFR is modeled for each cylinder as $\mathrm{AFR}=\mathrm{AFR}_j$ with $\mathrm{AFR}_j = 6m_{\mathrm{cyl}_j}(1-F_{\mathrm{cyl}_j})/(W_f\Delta T)$ and it is also sampled before the SOI for control purposes.

2.2 Intake Manifold States. Accordingly, for the intake manifold the mass and pressure state equations are defined as

$$dm_i/dt = W_c - \sum_{j=1}^{6} W_{i,\mathrm{cyl}_j} + \sum_{j=1}^{6} W_{\mathrm{cyl}_j,i}, \quad (7)$$

$$\frac{dp_i}{dt} = \frac{\gamma R}{V_i}\left[T_cW_c - T_i\sum_{j=1}^{6} W_{i,\mathrm{cyl}_j} + T_{\mathrm{cyl}_j}\sum_{j=1}^{6} W_{\mathrm{cyl}_j,i}\right]. \quad (8)$$

Following the same procedure with the cylinder state equations, the burned gas fraction in the intake manifold is defined as

$$dF_i/dt = \left(\sum_{j=1}^{6}(W_{\mathrm{cyl}_j,i}(F_{\mathrm{cyl}_j} - F_i)) - F_iW_c\right) \Big/ m_i. \quad (9)$$

2.3 Exhaust Manifold States. Similarly, the front exhaust manifold dynamics are represented by the following state equations:

$$dm_{e_f}/dt = \sum_{j=1}^{3} W_{\mathrm{cyl}_j,e_f} - \sum_{j=1}^{3} W_{e_f,\mathrm{cyl}_j} - W_{e_f,e_c}, \quad (10)$$

$$dp_{e_f}/dt = \gamma R\left(\sum_{j=1}^{3} T_{\mathrm{cyl}_j}W_{\mathrm{cyl}_j,e_f} - \sum_{j=1}^{3} T_{e_f}W_{e_f,\mathrm{cyl}_j} - T_{e_f}W_{e_f,e_c}\right) \Big/ V_{e_f}, \quad (11)$$

$$dF_{e_f}/dt = \left(\sum_{j=1}^{3}(W_{\mathrm{cyl}_j,e_f}(F_{\mathrm{cyl}} - F_{e_f})) + (W_{e_c,e_f}(F_{e_c} - F_{e_f}))\right) \Big/ m_{e_f}. \quad (12)$$

The state equations for the rear exhaust manifold are developed in the same manner with the ones for the front exhaust manifold. Equally, the state equations for the collector manifold are defined as

$$dm_{e_c}/dt = W_{e_f,e_c} - W_{e_c,e_f} + W_{e_r,e_c} - W_{e_c,e_r} - W_t, \quad (13)$$

$$dp_{e_c}/dt = \gamma R(T_{e_f}W_{e_f,e_c} - T_{e_c}W_{e_c,e_f} + T_{e_r}W_{e_r,e_c} - T_{e_c}W_{e_c,e_r} - T_{e_c}W_t)/V_{e_c}, \quad (14)$$

$$dF_{e_c}/dt = (W_{e_f,e_c}(F_{e_f} - F_{e_c}) + W_{e_r,e_c}(F_{e_r} - F_{e_c}))/m_{e_c}. \quad (15)$$

2.4 Turbocharger Dynamics. The turbocharger state equation is based on the conservation of energy on the turbocharger shaft, and consists of the rate of change of the turbocharger speed N_{tc}

$$dN_{\mathrm{tc}}/dt = (P_t - P_c)/(I_{\mathrm{tc}}N_{\mathrm{tc}}) \quad (16)$$

where P_t is the turbine power, P_c is the compressor power, and I_{tc} is the mass polar moment of inertia of the turbocharger. P_t and P_c are calculated based on a real adiabatic process and steady-state data provided by the turbocharger manufacturer. We neglect the effects of pulsating flow to turbocharger efficiency.

In particular, turbine maps f_{t_w} and f_{t_η} are used to determine the mass air flow W_t and the efficiency η_t. Both turbine maps are functions of the pressure ratio r_t across the turbine and the turbocharger speed N_{tc} after it has been normalized and corrected for variations in the exhaust temperature and pressure

$$P_t = W_tc_p\eta_tT_{e_c}(1-(1/r_t)^{(\gamma-1)/\gamma}), \quad (17)$$

$$W_t = f_{t_w}(N_{\mathrm{tc}}, T_{e_c}, r_t), \quad (18)$$

$$\eta_t = f_{t_\eta}(N_{\mathrm{tc}}, T_{e_c}, r_t), \quad (19)$$

$$r_t = p_{e_c}/p_0, \quad (20)$$

where p_0 is the ambient pressure and c_p is the specific heat capacity for constant pressure.

Similarly, using the data from the compressor maps we obtain the following compressor characteristics:

$$P_c = W_cc_pT_0(r_c^{(\gamma-1/\gamma)} - 1)/\eta_c, \quad (21)$$

$$W_c = f_{c_w}(N_{\mathrm{tc}}, T_0, r_c), \quad (22)$$

$$\eta_c = f_{c_\eta}(N_{\mathrm{tc}}, T_0, r_c), \quad (23)$$

$$r_c = p_i/p_0, \quad (24)$$

where T_0 is the temperature before the compressor, f_{cw} is the compressor map for mass flow, and $f_{c\eta}$ is the map for the compressor efficiency η_c. Both of these maps are functions of normalized and corrected turbocharger speed and the pressure ratio across the compressor. Detailed validation is shown in Refs. [12], [13], and [15].

2.5 Heat Release Modeling. The apparent fuel burn rate W_{afb} in kilograms per second (kg/s) for all cylinders ($W_{\mathrm{afb}}=W_{\mathrm{afb}_j}$) is calculated using an approximation of the heat released during the premixed and the diffusion period of the combustion, and is identified based on the cylinder pressure data and Eq. (2)

$$W_{\mathrm{afb}} = (\gamma p_{\mathrm{cyl}}(dV_{\mathrm{cyl}}/dt) + V_{\mathrm{cyl}}(dp_{\mathrm{cyl}}/dt))/(Q_{\mathrm{lhv}}(\gamma-1)) \quad (25)$$

where the cylinder volume V_{cyl} is the function of crank angle θ, the ratio of specific heats, γ, is assumed to be constant throughout the cycle, and Q_{lhv} is the lower heating value of light duty Diesel fuel. We use the crank angle resolved trajectories of the apparent fuel burnt W_{afb} and two functions for the premixed and the diffusive burning based on [10]

$$W_{\mathrm{afb}} = \max(W_{\mathrm{afb}}^{d^*}, W_{\mathrm{afb}}^{p^*}), \quad (26)$$

$$W_{\mathrm{afb}}^{d^*} = C_dk_{d2}(k_{d1}+1)\theta_d^{k_{d1}}\exp(-k_{d2}\theta_d^{(k_{d1}+1)}), \quad (27)$$

$$W_{\mathrm{afb}}^{p^*} = C_pk_{p2}k_{p1}(1-\theta_p^{k_{p1}})^{(k_{p2}-1)}\theta_p^{(k_{p1}+1)}, \quad (28)$$

where the variables $\theta_d=(\theta-\theta_{\mathrm{soc}})/\Delta\theta_d$ and $\theta_p=(\theta-\theta_{\mathrm{soc}})/\Delta\theta_p$ are defined over each combustion mode. To simplify the data fitting

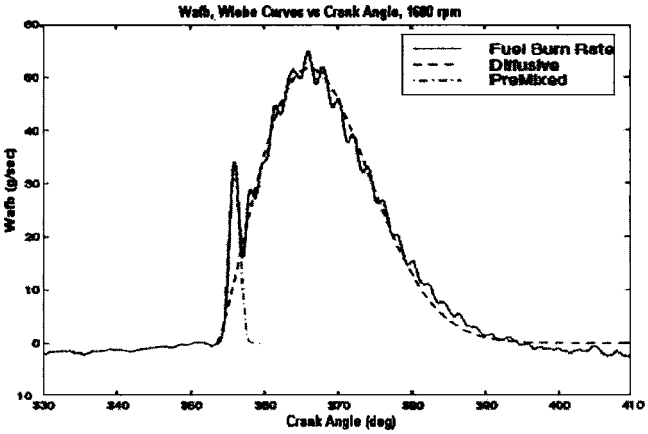

Fig. 3 Apparent fuel burn rate from experimental data and model prediction vs crank angle

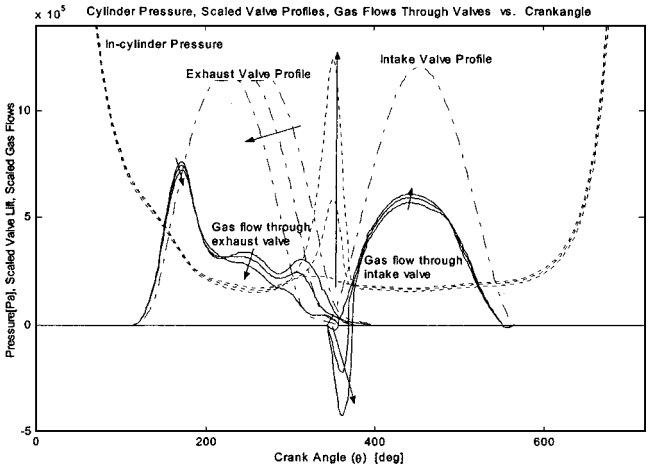

Fig. 4 Quasi-static in-cylinder pressure, valve profiles, and gas flows through valves (scaled) vs crank angle (°)

we assume that both premixed and diffusive combustion start at the same time, i.e., at the start of combustion

$$\theta_{\text{soc}} = \theta_{\text{soi}} + \Delta\theta_0. \tag{29}$$

Using the nonlinear optimization toolbox in Matlab we identify the six parameters (C_i's and k_{ij}'s), the two combustion mode durations $\Delta\theta_d$ and $\Delta\theta_p$, and the ignition delay $\Delta\theta_0$ for ten speeds and three loads. The identified values are then regressed on fueling level and engine speed. A good compromise between data fitting and small prediction errors is achieved with a polynomial (2^{nd} order in fueling level and 1^{st} order in engine speed) although special attention might be required in the future to obtain a minimal parameterization. Figure 3 shows the validation of the apparent fuel burnt rate. In the calculation of W_{afb}, we have coupled the heat losses through the walls H_{ht} and so the integral of the apparent fuel burn rate over a cycle is less than the mass fuel injected in the cylinder

$$\int_0^{\Delta T}\left(\sum_{j=1}^{6} W_{\text{afb}_j} Q_{\text{lhv}} + H_{\text{ht}}\right)dt = \int_0^{\Delta T} W_f Q_{\text{lhv}} dt \Rightarrow \int_0^{\Delta T}\sum_{j=1}^{6} W_{\text{afb}_j} dt < W_f \Delta T. \tag{30}$$

The actual fuel burnt that is used in (5) and (6) is defined as the fuel burnt $\alpha_{f_j} W_{\text{afb}}$ using the scale α_{f_j}

$$\alpha_{f_j} = W_f \Delta T \Big/ \left(6\int_0^{\Delta T} W_{\text{afb}_j} dt\right) \geqslant 1 \quad \text{and}$$
$$\int_0^{\Delta T}\sum_{j=1}^{6} \alpha_{f_j} W_{\text{afb}_j} dt = W_f \Delta T = \int_0^{\Delta T}\sum_{j=1}^{6} W_{f\,\text{cyl}_j} dt. \tag{31}$$

2.6 Flow Equations. The quasi-steady relation of the air flow through a restriction is based on the assumptions of one-dimensional, steady, and compressible flow of an ideal gas [2]

$$W_{xy} = C_d A_v \Psi(p_x, T_x, p_u) \tag{32}$$

where W_{xy} is the mass air flow (kg/s) from volume x to volume y, C_d is the discharge coefficient, and A_v is the flow area of the valve or the constant orifices between the intake (or exhaust) manifold and the atmosphere. The term Ψ is the standard orifice flow function (Eqs. (C.8) and (C.9) in Ref. [2]) that depends on the downstream pressure, p_y, the upstream pressure, p_x, and temperature, T_x. If the upstream pressure becomes smaller than the downstream pressure $p_x \leqslant p_y$, then $W_{xy}=0$ and W_{yx} becomes nonzero according to Eq. (32).

3 Variable Valve Timing Approach

To introduce the EVC capability, we express the exhaust valve area, A_v, of Eq. (32) as a function of EVC and crank angle degrees. The maximum allowable EVC advance is 50 deg. We use a variable step solver (ODE23s stiff Rosenbrock) from the simulation parameter options of Matlab/Simulink with tolerances of $1e^{-4}$. These simulation parameters are chosen to avoid numerical integration problems but result in slow simulation, namely 17 s per engine cycle with 256 MB random access memory, P3 800 MHz computer.

Figure 4 shows simulation results sampled every two carnkangle degrees. Specifically, Fig. 4 shows three values of EVC timing resulting in three different values for iEGR. The direction of the arrows indicates the progression of intake and exhaust flows over the range of changing EVC. The first curve in each progression (as indicated by the direction of each arrow) corresponds to the original exhaust valve profile, with EVC at 404 deg after the Top Dead Center (TDC). The EVC is then advanced about 25 deg and then 50 deg. Early EVC closing increases the exhaust gas trapped in the cylinder and causes recompression at the end of the exhaust stroke. The resulting high in-cylinder pressure causes some amount of residual gas to flow into the intake manifold. When the cylinder pressure value drops below the intake manifold pressure value, induction begins thereby augmenting iEGR that can be regulated with a single actuator, EVC.

3.1 Cycle-Sampled or Averaged Behavior. The high order nonlinear crank angle resolved dynamical model enhances our understanding and is used to model the crank angle resolved system behavior. The controlled variable, EVC, is a cycle-resolved variable and thus a cycle-averaged model-based controller is required. The performance variables of interest are torque (Tq), AFR, and burned gas fraction (F_{cyl}). Conventional production sensors provide the intake manifold pressure (p_i).

We create a series of linear and cycle-averaged models by processing the crank angle resolved data to obtain the input-output cycle-sampled behavior. The output data from the simulation is recorded every 2 crank angle degrees. The cycle-averaged intake manifold pressure and torque are obtained as arithmetic averages of the crank angle resolved data. These arithmetic average values are assigned to the whole cycle period. The in-cylinder burned gas fraction (F_{cyl}) is sampled for every cylinder and every cycle just before the start of injection. The value of the burned gas fraction before injection corresponds to the charge dilution which affects the combustion characteristics, and thus, the generated emissions. In-cylinder AFR cycle-resolved sampling is similarly performed;

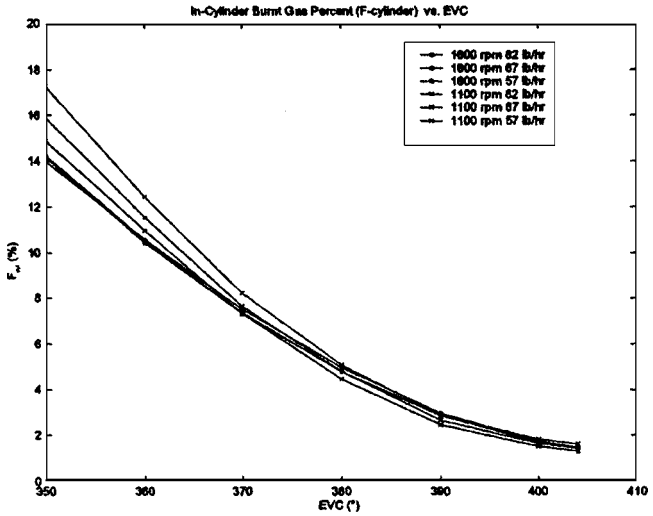

Fig. 5 Steady state maps for in-cylinder burned gas fraction vs EVC

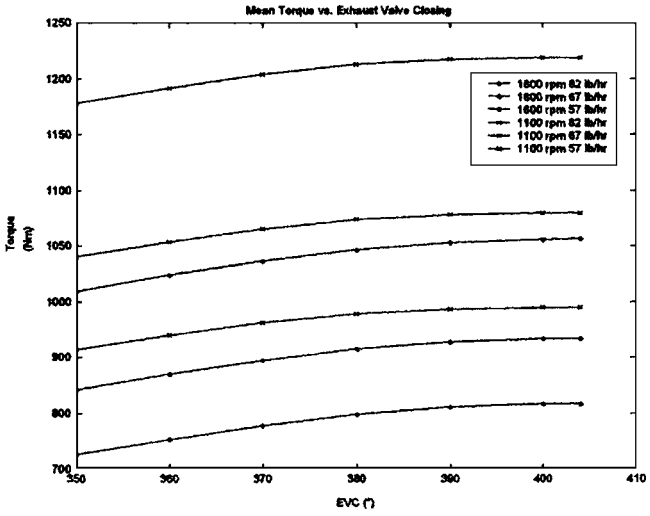

Fig. 7 Steady state maps for mean torque vs EVC

the sampling scheme captures the AFR based on the sampled total and burned gas mass just before the injection starts and uses this as the relevant value until the next cycle.

Simulation results for different speeds and loads show a consistent correlation between advanced EVC and increased burned gas fraction. As Fig. 5 shows, it is possible to increase the burned gas fraction in the cylinder up to 14%. This increase in the burned gas fraction is followed by relatively low degradation of AFR and mean torque (Figs. 6 and 7). For extreme values of advanced EVC (50°) during medium speed-medium load conditions, AFR drops below the acceptable limits for visible smoke (smoke limit $AFR_{sl}=18$). During these operating conditions, effective iEGR can be achieved with a lower value of an advanced EVC, typically around 35°–40°. Figure 7 shows the degradation in the mean torque as a result of the recompression. However, even for excessively advanced EVC conditions (about 50°) the mean torque loss is around 5-9% whereas the in-cylinder burned gas fraction is increased up to 14–18%. This loss in terms of torque might be tolerable for most operating conditions. The inlet manifold pressure decreases for advanced EVC as Fig. 8 shows. This occurs because the exhaust mass trapped in the cylinder reduces the energy transmitted from the exhaust gas to the turbine, and thus reduces the TC speed. Consequently, this drop in the boost pressure amplifies the effects of the recompression and compounds to a lower torque output as shown in the steady state mean torque maps.

Using these steady-state maps, look-up tables for the engine management system can be prepared in order to adjust the engine controller outputs, fueling rate, and EVC timing according to the inputs, pedal position, and engine speed [5]. Table 1 shows the optimum EVC values that maximize burned gas fraction while satisfying steady-state AFR=30 for different fueling levels at 1600 rpm. Table 1 shows the inlet manifold pressure, mass flow rate, and burned gas fraction associated with the optimum EVC at each fueling rate. We also report the torque loss associated with the optimum EVC selection. Note that the optimum EVC is selected based on emissions criteria and not torque output, because the driver typically adjusts the pedal position, and consequently the fueling rate to achieve the desired torque. Note also that at high fueling rates the optimum EVC slowly returns to nominal (zero EGR) values enabling the delivery of the maximum engine torque. A feedforward map based on the look-up Table 1 is augmented by a feedback controller designed in the following sections to improve the transient response and to robustify the closed loop system.

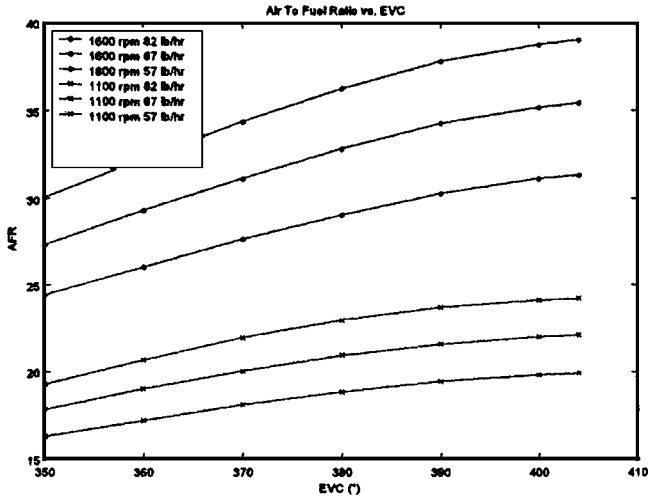

Fig. 6 Steady state air to fuel ratio vs EVC

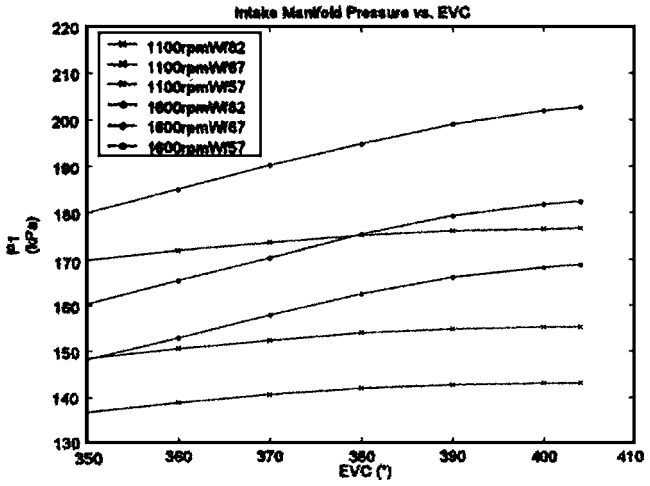

Fig. 8 Steady state inlet manifold pressure vs EVC

Table 1 Optimal set points for 1600 rpm

Fuel rate	Optimum EVC (deg)	Inlet manifold pressure (p_i) (kPa)	Compressor mass flow rate (w_c) (g/s)	% torque loss compared to zero EGR	% burned gas fraction in cylinder (F_{cyl})
82 lb/h (10.33 g/s)	390°	199	304	9	14
67 lb/h (8.44 g/s)	365°	168	238	6	9
57 lb/h (7.18 g/s)	350°	148	197	2	3

3.2 Identification of Linear Input/Output Model. In order to design a cycle-based feedback controller we perform multivariable linear system identification around a series of operating points. The input/output behavior includes all the system inputs, namely, W_f and EVC. The identification also includes all the system outputs, namely, $Z=[Tq, \text{AFR}]$ as the performance variables, $y=[p_i]$ as the measured outputs resulting in a two-input, three-output system. To identify the linear system, we use step changes in W_f and EVC and sample the cycle-resolved dynamic response. The cycle-resolved data are then imported into the Matlab System Identification Toolbox, and the multi-input multi-output linear system parameters are identified using state space parametric model estimation technique N4SID. Identification is performed around the operating points corresponding to 1600 rpm, 57 lb/h with EVC set to the original value of 404 deg ATDC and two advanced values, 350 and 395 deg. These points cover the dynamic range of the EVC as an actuator, thereby providing information necessary to evaluate the suitability of the actuator approach and design a controller that accounts for the engine dynamics. A third order model captures the dynamical behavior of the input-output behavior at all the operating points allowing controller design at each operating point and gain scheduling if it is deemed necessary. The three states must correspond to the dominant dynamics associated with the turbocharger, the intake manifold, and the exhaust manifold, although this has not been verified explicitly by perturbation analysis. The identification results are shown in Fig. 9. The two lines are indistinguishable indicating the good match between the identified and the crank angle resolved model.

The identified models at the three operating points have very similar frequency responses with notable differences only in their direct current (dc) gain as shown in the Bode magnitude plots in Fig. 10. Since integral control will account for the modeling errors in dc gain, we continue the control design using the identified model at EVC=395 deg. As shown later in Fig. 14, the model-based controllers designed based on one nominally identified model managed successfully large fuel step changes associated with a torque increase of 200 N m. Note here that the identified system might not be valid for frequencies higher than 10 rad/s that corresponds to the cycle sampling frequency at 1600 rpm.

Before the control design we apply input/output scaling in order to avoid numerical problems and capture the physical range of actuator authority and output significance. The output scale is $T_z=\text{diag}([1/100, 1/7])$, the measurement scale is $T_y=1/10{,}000$, and the input scaling is $T_u=\text{diag}([1/0.003, 1/50])$. The state space representation of the scaled identified system is

$$\dot{x}=Ax+Bu, \quad \dot{x}=\begin{bmatrix} -1.571 & 0.307 & 2.545 \\ 6.510 & -25.710 & -33.058 \\ 0.813 & 1.023 & -14.095 \end{bmatrix}x + \begin{bmatrix} -9.610 & -7.691 \\ 51.085 & -9.364 \\ 3.885 & 6.861 \end{bmatrix}\begin{bmatrix} W_f \\ \text{EVC} \end{bmatrix} \tag{33}$$

with inputs $u^T=[u_1\ u_2]=[W_f\ \text{EVC}]$ and performance variables $z^T=[z_1 z_2]$

$$z=C_z x+D_z u, \quad \begin{bmatrix} T_q \\ \text{AFR} \end{bmatrix}=\begin{bmatrix} -0.01 & 0.002 & -0.06 \\ 0.04 & -0.97 & -0.23 \end{bmatrix}x + \begin{bmatrix} 3.23 & 1.64 \\ -0.35 & 0.12 \end{bmatrix}\begin{bmatrix} W_f \\ \text{EVC} \end{bmatrix} \tag{34}$$

and measurements $y=p_i$

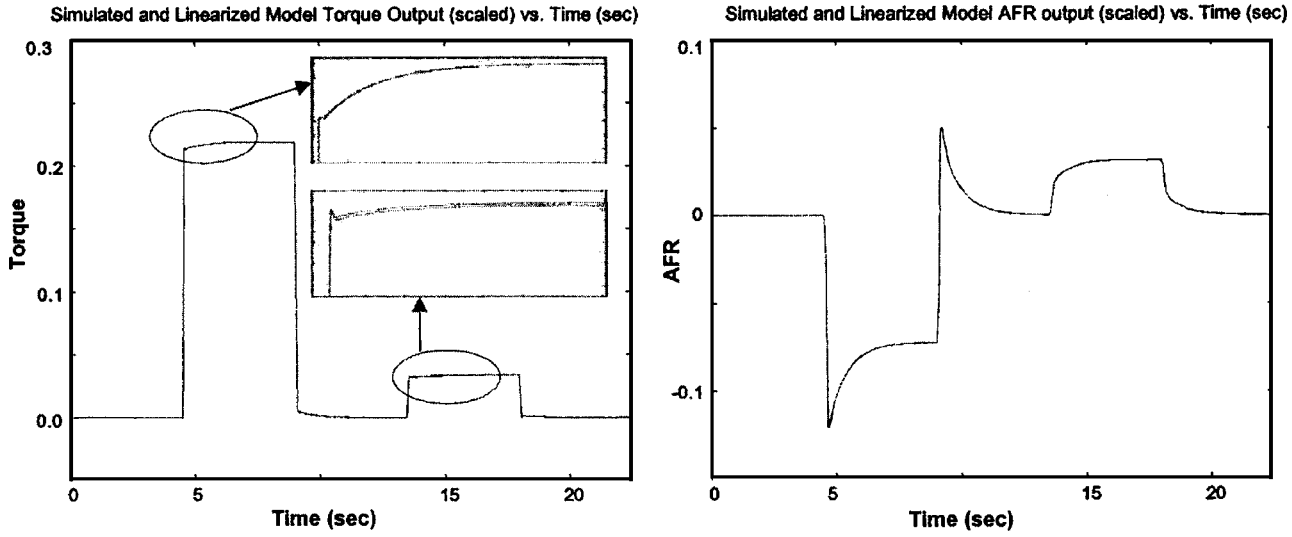

Fig. 9 System identification results (W_f step up/down, EVC step up/down, respectively)

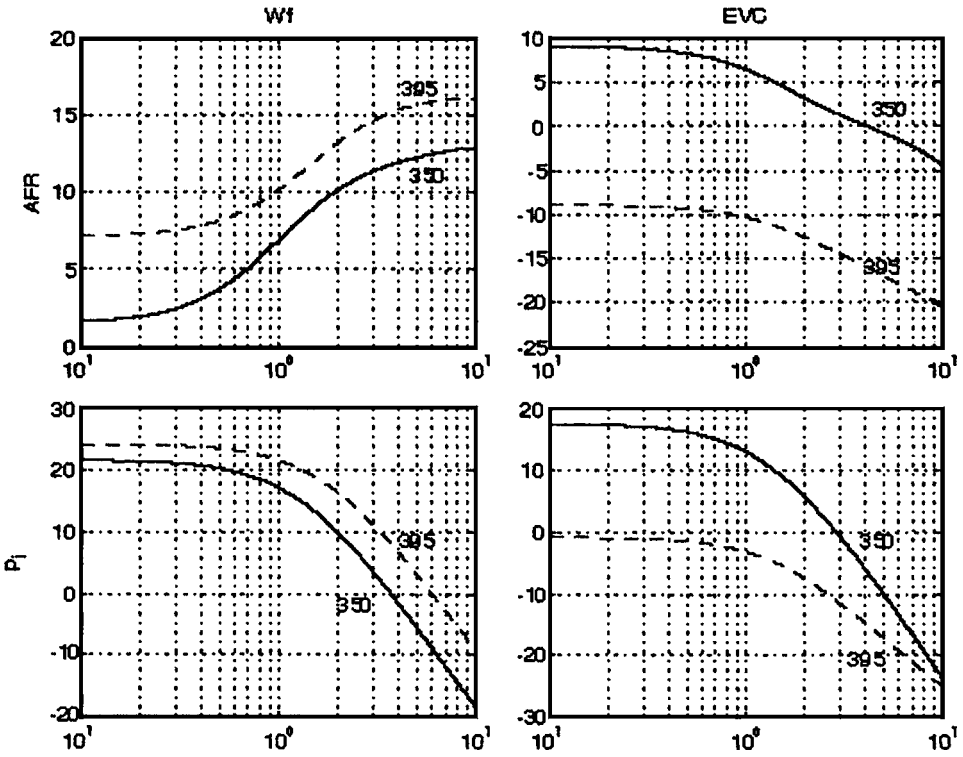

Fig. 10 Bode magnitude plots in dB and rad/s of the linear identified systems at 1600 rpm, 57 lb/h with EVC 350° (solid line) and 395° (dash line).

$$y = C_y x + D_y u, \quad y = [-0.47\ 0.002\ -0.12]x + [0.099\ 0.014]\begin{bmatrix} W_f \\ \text{EVC} \end{bmatrix}. \tag{35}$$

The individual input/output transfer functions of $Z = G_z U = [C_z(sI - A)^{-1}\boldsymbol{B} + D_z]U$ and $Y = G_y U = [C_y(sI - A)^{-1}B + D_y]U$ are also defined as

$$\begin{bmatrix} z_1 \\ z_2 \end{bmatrix} = \begin{bmatrix} G_{z11} & G_{z12} \\ G_{z21} & G_{z22} \end{bmatrix}\begin{bmatrix} u_1 \\ u_2 \end{bmatrix} \quad \text{and} \quad y = [G_{y1}\ G_{y2}]\begin{bmatrix} u_1 \\ u_2 \end{bmatrix}. \tag{36}$$

All variables above are considered as perturbations from the nominal values, but for simplicity we do not employ a different notation.

4 Controller Design

The goal of the controller design is to achieve high burned gas fraction in the cylinder while satisfying the driver's torque demand and the smoke-limited AFR constraints. The set points derived in the previous section show that high F_{cyl} is achieved when the EVC is controlled to maintain a constant AFR=30 for all fueling rates at 1600 rpm. At lower engine speed (e.g., N =1100 rpm) the overall AFR level is low, thus, the EVC can be controlled to maintain a low but feasible AFR=20. We assume here that engine speed varies slower than the engine variables in consideration. We, thus, focus at the control design during constant engine speed with the intent to extend our results for varying engine speeds as in Ref. [14] in the future. Torque is primarily controlled by the commanded fuel flow, W_f, although the EVC can now affect engine torque in a significant way. Similarly, the EVC and W_f affect the AFR resulting in a coupled two-input two-output system. Although the state space representation in (33)–(35) or the input-output representation in (36) can be used to synthesize a multivariable controller that coordinates both the EVC and W_f, we wish to maintain a modular control architecture that utilizes the conventional fuel-governor and allow the seamless addition of an EVC controller.

In nonidle operation, conventional electronic fuel-governors are based on pedal position. Specifically, the pedal position is read by the engine computer and translated to acceleration demand or torque request that is achieved by different fueling levels at different engine speeds. The fuel command is controlled to avoid abrupt torque changes and consequently prevent high frequency excitation to the driveline. We assume that a torque response that achieves a good compromise between driveline excitation and drivability requirements corresponds to a first order lag with time constant of 0.5 s. Sometimes very fast torque response is desired to damp driveline oscillations induced from other powertrain disturbances [16]. The time constant assumption will influence the tunable parameter of all three controllers presented in this paper. It is important to note here that neither the controller architecture nor the procedure for tuning the controller parameters should change by assuming a slower or a faster desired torque response.

In the modular W_f-EVC controller configuration, increased W_f increases torque but causes an abrupt decrease in the AFR acting as a disturbance to the AFR. A well designed EVC controller needs to reject the fuel disturbance to the AFR by adjusting the air in the cylinder. The EVC controller must regulate the AFR fast to its nominal value and avoid an EVC overshoot. Both requirements are hard to achieve, since fast AFR regulation might require a lead EVC controller, which causes an EVC overshoot during a step change in an AFR error in a feedback configuration. The nonovershoot requirement is imposed by the EVC-torque interaction rather than by actuator constraints. Specifically, an overshoot in the EVC will cause an overshoot in torque with potential detrimental drivability implications. The EVC controller thus needs to regulate the AFR during fueling commands and minimize its effects on torque, so that the fuel-torque loop can be designed independently or remain unchanged if the EVC is an add-on device.

In the following sections we consider three control schemes for

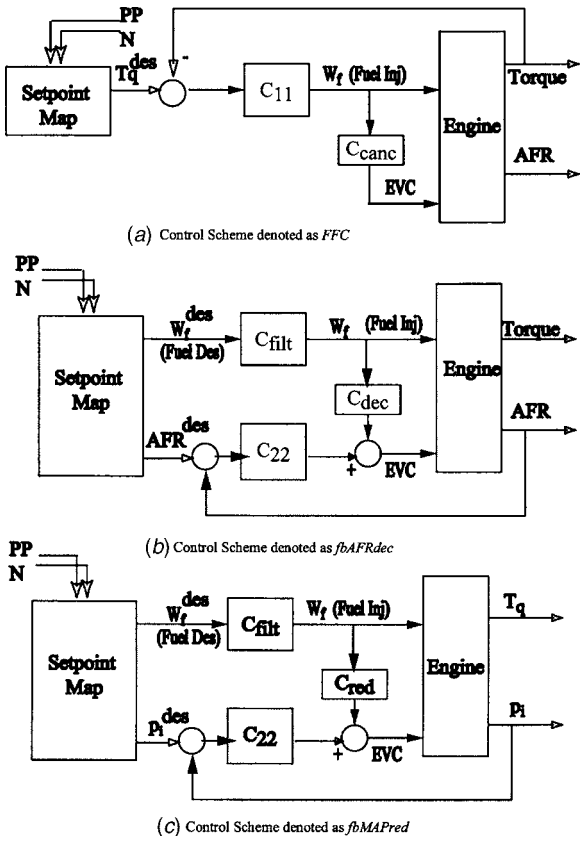

Fig. 11 Three control architectures based on different sensor sets

the EVC controller as illustrated in Fig. 11. We first investigate if the EVC can achieve perfect AFR control during fuel steps by completely canceling the effect of the fuel to the AFR. We show that the cancellation controller is possible based on the linear low-order identified dynamic model and the fact that the fuel command is known or can be communicated without a delay to the EVC controller. The ideal-cancellation EVC scheme based on the dynamic feedforward controller is integrated with an integral based controller for the fuel-torque (W_f-T_q) loop. The fuel-torque controller is needed for a time-wise monotonic torque response with 0.5 s time lag, while the EVC aggressively regulates the AFR with the cancellation controller. This control scheme is denoted as feedforward cancellation "FFC" and is shown in Fig. 11(*a*). The practical value of the FFC control scheme is limited due to (i) the lack of in-vehicle torque sensors, (ii) the existence of potential delays in the fuel-EVC controller communication or EVC actuator, and (iii) the sensitivity of the cancellation EVC controller to engine and component aging. Despite its limitations this scheme provides insight on the commands that can achieve perfect control of torque and AFR and provides a benchmark for the design of two other control schemes shown in Figs. 11(*b*) and 11(*c*).

Measurement avaliability and realizability of the high frequency FFC controller dictate the two control designs in Figs. 11(*b*) and 11(*c*). In both control schemes we filter the desired fuel command for a torque response of 0.5 s time lag and tune a two degrees of freedom (2DOF) EVC controller for the AFR regulation. The EVC controller in Fig. 11(*b*) denoted as "*fbAFRdec*" is based on AFR feedback and a static feedback and a static feedforward controller (dc-gain of the FFC) that decouples the AFR from fuel at steady state. Finally, we show that intake manifold pressure measurements p_i, also known as manifold absolute pressure (MAP), can also be used in an EVC controller if integrated with a dynamic feedforward controller that decouples the AFR

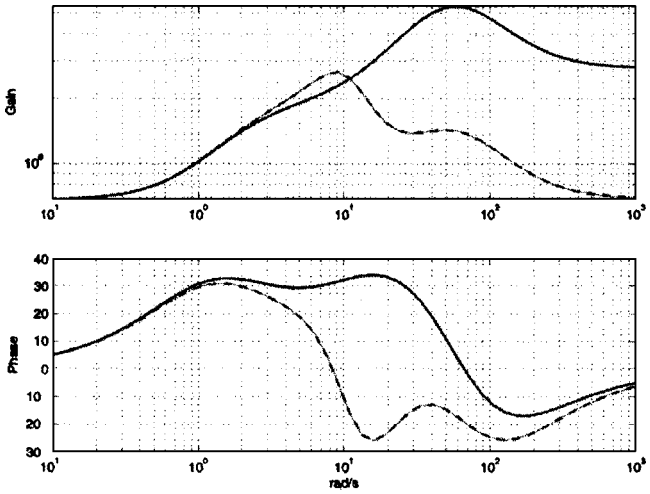

Fig. 12 Bode plot for the ideal-cancellation controller (C_{canc} solid line) and reduced-cancellation controller (C_{red} dash line)

from fuel. This third scheme is denoted as "*fbMAPred*" and shown in Fig. 11(*c*).

4.1 Ideal Cancellation Controller. A feedforward controller, C_{canc}, that cancels completely the AFR excursions during fueling changes can be derived from

$$\mathrm{AFR} = G_{z21}W_f + G_{z22}\mathrm{EVC} = 0 \Rightarrow \mathrm{EVC} = \underbrace{-(G_{z22})^{-1}G_{z21}}_{C_{canc}}W_f \tag{37}$$

where $G_{z22} = (s+2.16)((s+48.16)^2+27.9^2)/((s+1.33)((s+20.02)^2+0.75^2))$ and $G_{z22} = (s+0.77)(s+12.34)(s+174.53)/((s+1.33)((s+20.02)^2+0.75^2))$ are calculated from (36).

The cancellation controller is possible because G_{z22} does not have any nonminimum phase zeros or delays. The frequency response of the cancellation controller is shown by the solid line in Fig. 12. The dash line corresponds to a modified cancellation controller discussed in Sec. 4.3. Closed loop simulation of the ideal cancellation controller with the linear engine dynamics of Eq. (36) shows that the AFR is regulated despite changes in fueling W_f as shown with the solid line in Fig. 13. This perfect AFR regulation is achieved by a very fast EVC control. Note here that a fast EVC retardation allows more air in the cylinder by reducing the iEGR. This allows tight AFR regulation but increases torque at the same time.

To ensure a monotonically increasing torque response during increasing fuel command independently of the EVC activity, we design a feedback controller for fuel based on torque measurement that completes the FFC scheme shown of Fig. 11(*a*). Consider the reduced order model of the dynamics between fuel W_f and torque T_q based on the upper and left transfer function in Eq. (36)

$$G_{z11} = (s^2 + 40s + 399.1)/(s^2 + 40s + 401.6). \tag{38}$$

.

The open loop pole and zero conglomeration of G_{z11} occur close to the frequency where the cycle-averaged model breaks down and it is a pure artifact of the MIMO identification. The fuel W_f to torque T_q dynamics can, thus, be simplified to

$$G_{z11} = 1. \tag{39}$$

Note that the unit gain is achieved with the I/O scaling applied in Sec. 3.2. We choose a simple integral controller

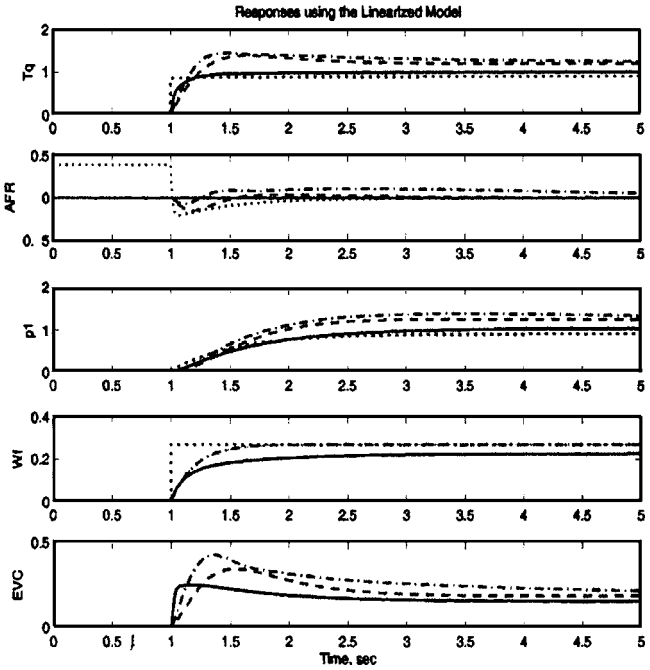

Fig. 13 Response of linear closed loop schemes: FFC in solid line, *fbAFRdec* in dash line, *fbMAPred* in dash-dot line, and conventional engine linear response with fixed EVC=404° in dot line. All graphs show deviations from the nominal values where linearization was performed.

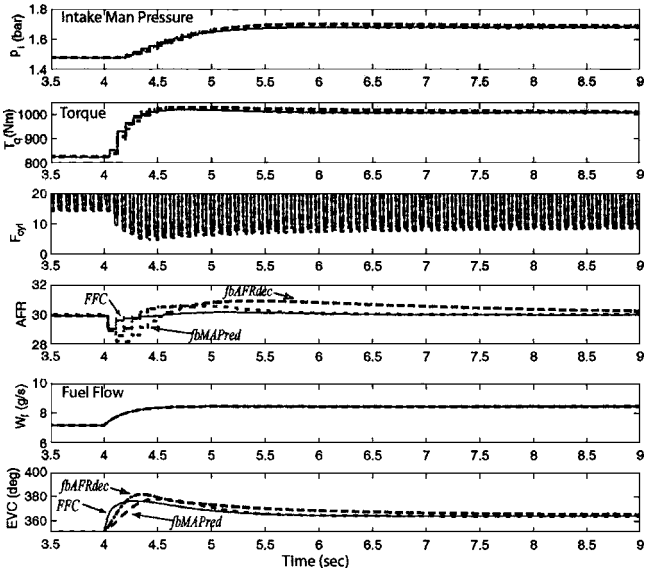

Fig. 14 Nonlinear full order closed loop system response for FFC in solid line, *fbAFRdec* in dash line, and *fbMAPred* in dash-dot line

$$C_{11} = 2/s \tag{40}$$

because it corresponds to a linear scaled closed loop torque response of a first order lag with time constant of 0.5 s when the EVC is fixed as can be seen by the upper feedback loop of Fig. 9(*a*)

$$T_q/T_q^{\text{des}} = (1 + G_{z11}C_{11})^{-1}G_{z11}C_{11} = (1 + 2/s)^{-1}2/s = 1/(0.5s + 1).$$

The solid line in Fig. 13 shows the simulation of the linear closed loop system with the FFC controller based on (37) and (40). Figure 13 shows with dotted line the conventional (fixed EVC) response of the linear identified engine model during a fuel step change for comparison. Other control schemes discussed in later sections are shown with dash and dash-dot lines. The T_q response resembles a first order lag with 0.5 s time constant and the AFR is always constant in the FFC scheme. This controller, although not practical, gives us insight to the coupling and coordination between the two actuators for a perfect AFR regulation [17]. Later in Fig. 14 (solid line) we apply the same controller in the full-order crank angle resolved model with minimum degradation of performance. Note here that although the cancellation controller is sensitive to modeling assumptions and uncertainties, it does not degrade the closed loop stability due to its feedforward structure.

4.2 Feedback Control Based on AFR Measurements. Since a T_q sensor is not readily available for vehicle applications, one has to implement the torque feedback based on an in-cylinder pressure measurement, such as peak pressure, or IMEP. Although in-cylinder pressure measurements are not entirely out of the question, they are very expensive and sensitive. We, thus, consider a filtered step change in W_f in response to a torque demand instead of a closed loop W_f command. In other words, we can emulate the smooth fueling command of the closed loop W_f-T_q by filtering an open loop fuel step change that is scheduled to achieve a desired steady state T_q response based on pedal position. Note here that the driver can act as an integrator by adjusting the pedal position if the desired torque or acceleration command is not met by the open loop fuel scheduling. The fueling filter time constant is chosen to be 0.5 s in order to match the closed loop response of the first design

$$C_{\text{flit}} = 1/(0.5s + 1). \tag{41}$$

Realizability based on the EVC actuator constraints and the validity of the cycle-averaged model bandwidth are then considered. The cancellation controller is reduced to a static feedforward cross-coupling term from fuel to the EVC

$$C_{\text{dec}} = C_{\text{conc}}(0) \tag{42}$$

by using the dc gain of the cancellation controller.

The feedforward EVC controller is augmented with a feedback controller based on the AFR measurement to complete the *fbAFRdec* control scheme shown in Fig. 11(*b*). In this control scheme we assume an ideal in-cylinder AFR measurement or accurate model-based estimators. Although such sensors or estimators are not typical in Diesel engines, the *fbAFRdec* control configuration provides insight on the benefits of accurate AFR knowledge for EVC feedback. We design a lead-lag controller with an integrator

$$C_{22} = 2.73(0.75s + 1)/(s(0.46s + 1)) \tag{43}$$

by first canceling the slowest pole and zero of G_{z22} and then tuning the dc gain of sC_{z22} so that the closed loop W_f to AFR exhibits small overshoot. Overshoot in the AFR corresponds to aggressive EVC retardation that can increase torque, and thus interact with the W_f-T_q response. The nonovershooting requirement results in a C_{z22} that cannot be fast enough to reject the W_f disturbance to the AFR without the feedforward term from Eq. (42). Due to the feedforward term C_{dec} that makes the EVC change instantaneously when fuel changes the EVC-AFR (lower) loop follows the W_f-T_q response. The linear feedback controller *fbAFRdec* in Fig. 11(*b*) with Eqs. (41)–(43) shows good T_q and AFR response even during high charge dilution (see dash line in Fig. 13). The total burned gas fraction is $F_{\text{cyl}}=11\%$ at nominal fueling level and decreases down to $F_{\text{cyl}}=8\%$ in order to maintain AFR=30 during the increase in fueling level. The conventional engine (dot line) operates at $F_{\text{cyl}}=1.5\%$ and AFR=[30−42] with EVC=404.

4.3 Feedback Control Based on Measured Intake Manifold Pressure. In this section we design an EVC control scheme when conventional engine measurements such as pressure (p_i) are

used. It is important to note here that in the TC Diesel engine p_i is a measurement that correlates well with the engine pumping rate and thus the AFR in the presence of a variable EVC. A one-to-one steady-state coupling between p_i and AFR is maintained due to the turbocharger interaction between the intake and exhaust manifolds. Specifically, the EVC affects the AFR directly through the captured F_{cyl} and indirectly through p_i (from EVC to p_e to turbine speed to compressor flow to p_i). However, p_i cannot capture the fast interaction between the EVC and AFR and thus, p_i cannot support a fast feedback loop. The open loop transfer function from the EVC to p_i, also called MAP, corresponds to a slow real dominant pole

$$G_{y2} = 1285/((s + 1.33)((s + 20)^2 + 0.56)) \tag{44}$$

For fast AFR regulation we rely on a 2DOF controller denoted as *fbMAPred* that uses a modification of the cancellation controller, Eq. (40), and a slow integrator on p_i measurement

$$\text{EVC} = (0.12/s)(p_i - p_i^{\text{des}}) + C_{\text{red}} W_f \tag{45}$$

where

$$C_{\text{red}} = C_{\text{canc}}(\omega_{n2}^2/\omega_{n1}^2)((s^2 + 2\zeta_1\omega_{n1}s + \omega_{n1}^2)/(s^2 + 2\zeta_2\omega_{n2}s + \omega_{n2}^2)). \tag{46}$$

We employ the dynamic feedforward C_{red} from W_f to EVC, which is a decoupler with reduced gain at high frequencies by filtering the high frequency (>10 rad/s) content of the cancellation controller. The Bode plot of the cancellation controller in Eq. (37) and the one with the reduced gain in Eq. (46) are shown in Fig. 12 with solid and dashed lines, respectively. The gain of the feedback term of (45) is again tuned so that the closed loop W_f to the EVC has a small overshoot. Recall that we need to avoid excessive overshoot on the EVC that might cause T_q overshoot or EVC saturation. Due to these stringent constraints on the feedback design, compound by the slow open loop EVC to AFR response shown in (44), we cannot avoid the dynamic feedforward (ideal-cancellation or reduced cancellation) altogether and instead use the static feedforward from (42).

The linear response of the *fbMAPred* controller is shown in Fig. 13 in a dash-dot line. The closed loop response achieves a smooth torque response with slightly more overshoot than the *fbAFRdec* control scheme. Both feedback controllers (*fbAFRdec* and *fbMAPred*) exhibit similar AFR excursions. The dynamic feedforward controller in the *fbMAPred* control scheme allows fast EVC responses during fuel changes despite the slow p_i response. We conclude that the modified cancellation feedforward with the slow integral controller achieve satisfactory response. Note that in the case of an unthrottled gasoline (SI or DI) engine cycle-resolved p_i is not meaningful for feedback because it is constant and equal to the atmospheric pressure. In the gasoline engine a UEGO or an EGO sensor can provide the appropriate measurement for AFR feedback control. In this case one should consider a modification of the *fbAFRdec* control scheme.

4.4 Closed Loop Nonlinear Simulations. The three control schemes are applied to the nonlinear full-order crank angle resolved TC Diesel engine model during a fuel step change from 57 to 67 lb/h (7.18–8.44 g/s) that corresponds to 200 N m increase in torque. This step corresponds to 20% of the maximum torque for this engine. The responses are shown in Fig. 14. Similar to Fig. 13 the solid line corresponds to the FFC control scheme, the dash line to the *fbAFRdec*, and the dash-dot to the *fbMAPred*. In the crank angle resolved simulation the W_f and the T_q response is similar for all the control schemes, whereas the EVC and the AFR responses differ. As the linear simulations in Fig. 13 indicated, the best AFR response is achieved with the cancellation controller in the FFC control scheme. However, the FFC control scheme cannot regulate perfectly the nonlinear AFR response due to the mismatch between the linear low-order identified and the nonlinear crank angle resolved model. Similar to the linear simulations, the AFR response of the *fbMAPred* controller is better than the one in *fbAFRdec* due to the dynamic feedforward controller.

All the control schemes result in similar responses in intake manifold pressure despite their differences in the EVC and AFR responses. The third plot in Fig. 14 includes the crank angle resolved cylinder burned gas fraction (F_{cyl}). The cycle-minimum value of F_{cyl} corresponds to the sampled-value when the intake valve closes and remains constant during the compression phase. F_{cyl} then increases by the amount of fuel and air burnt during combustion. Recall here that the F_{cyl} before the combustion is responsible for the NO_x reduction and the calculation of the in-cylinder AFR. As Fig. 14 shows the cycle-minimum value of F_{cyl} remains always greater than 5% during a transition from the steady state values of 14%–9%. In comparison, the conventional TC Diesel engine with fixed EVC=404° operates with almost zero F_{cyl}.

5 Conclusions

We show using simulations that the EVC can be used for management of iEGR in turbocharged Diesel engines. Using a combination of static and dynamic feedforward augmented with simple proportional integral controllers we achieve fast regulation of in-cylinder AFR in an effort to reduce visible smoke during torque accelerations. The difficulty in the control tuning arises mostly from the fact that the EVC affects both the AFR and Tq. Coordination of fueling (W_f) and EVC is thus required. We show here the methodology for achieving the desired coordination given AFR or intake manifold pressure sensor.

Nomenclature

General Engine Parameters

V_{cyl} = 0.002 Cylinder disp. volume (m^3)
N_{cyl} = 6 Number of cylinders

Valve Parameters

IVO = 336 Intake valve opening (deg)
IVC = 580 Intake valve closing (deg)
EVO = 116 Exhaust valve opening (deg)

Geometrical Parameters

Vi = 4.918*e*-03 Intake manifold volume (m^3)
V_{e_f} = 1.2052*e*-3 Front exh. manifold vol. (m^3)
V_{e_r} = 1.2768*e*-3 Rear exh. manifold vol. (m^3)
V_{e_c} = 2.448*e*-03 Exhaust collector manifold volume (m^3)

Constants

R = 287 Gas constant [J/(kg K)]
γ = 1.37 Ratio of specific heats
AFRs = 14.5 Stoichiometric air-to-fuel (mass) ratio

References

[1] Guzzella, L., and Amstutz, A., 1998, "Control of Diesel Engines," IEEE Control Syst. Mag., **18**(2), pp. 53–71.
[2] Heywood, J. B., 1988, *Internal Combustion Engine Fundamentals*, McGraw-Hill, New York.
[3] Najt, P., and Foster, D., 1983, "Compression-Ignited Homogeneous Charge Combustion," SAE paper 830264.
[4] Thring, R. H., 1989, "Homogeneous-Charge Compression-Ignition (HCCI) Engines," SAE paper 892068.
[5] Stefanopoulou, A., Kolmanovsky, I. V., and Freudenberg, J. S., 2000, "Control of Variable Geometry Turbocharged Diesel Engines for Reduced Emissions," IEEE Trans. Control Syst. Technol., **8**(4), pp. 733–745.
[6] Edwards, S. P., Frankle, G. R., Wirbeleit, F., and Raab, A., 1998, "The Potential of a Combined Miller Cycle and Internal EGR Engine for Future Heavy Duty Truck Applications," SAE paper 980180.
[7] Dekker, H., and Sturm, W., 1996, "Simulation and Control of a HD Diesel Engine Equipped with new EGR Technology," SAE paper 960871.
[8] Nelles, O., Fink, A., and Isermann, R., 2001, "Local Linear Model Trees (LILIMOT) Toolbox for Nonlinear System Identification," *Proceedings 12th IFAC Symposium on System Identification*, Vol. 3, pp. 845–50.

[9] Kao, M., and Moskwa, J. J., 1995, "Turbocharged Diesel Engine Modeling for Nonlinear Engine Control and Estimation," ASME J. Dyn. Syst., Meas., Control **117**, pp. 20–30.
[10] Watson, N., and Janota, M. S., 1982, *Turbocharging the Internal Combustion Engine*, Wiley Interscience, New York.
[11] Jankovic, M., Frischmuth, F., Stefanopoulou, A. G., and Cook, J. A., 1998, "Torque Management of Engines with Variable Cam Timing," IEEE Control Syst. Mag. **18**, pp. 34–42.
[12] Moklegaard, L., Druzhinina, M., and Stefanopoulou, A., 2001, "Compression Braking for Longitudinal Control of Commercial Heavy Vehicles," PATH Report UCB-ITS-PRR-2001-11.
[13] Moklegaard, L., Stefanopoulou, A. G., and Schmidt, J., 2000, "Transition from Combustion to Compression Braking," SAE 2000-01-1228, SAE World Congress.
[14] Druzhinina, M., Stefanopoulou, A. G., and Moklegaard, L., 2002, "Adaptive Continuously Variable Compression Braking Control for Heavy-Duty Vehicles," ASME J. Dyn. Syst., Meas., Control **124**(3), pp. 406–414.
[15] Moklegaard, L., Druzhinina, M., and Stefanopoulou, A. G., 2001, "Brake Valve Timing and Fuel Injection: a Unified Engine Torque Actuator for Heavy-Duty Vehicles," Veh. Syst. Dyn., **36**(2-3), pp. 179–201.
[16] Kiencke, U., and Nielsen, L., 2000, *Automotive Control Systems*, Springer-Verlag, New York.
[17] Skogestad, S., and Postlethwaite, I., 1996, *Multivariable Feedback Control: Analysis Design*, Wiley, New York.